Breaking Rank Bottlenecks
in Knowledge Graph Completion

Samy Badreddine[1,2,3]   **Emile van Krieken**[4,*]   **Luciano Serafini**[2,3,*]

[1]Sony AI   [2]Fondazione Bruno Kessler   [3]University of Trento   [4]University of Edinburgh

Samy.Badreddine@sony.com
Emile.van.Krieken@ed.ac.uk
Luciano.Serafini@fbk.eu

Abstract

Many Knowledge Graph Completion (KGC) models, despite using powerful encoders, rely on a simple vector-matrix multiplication to score queries against candidate object entities. When the number of entities is larger than the model's embedding dimension, which in practical scenarios is often by several orders of magnitude, we have a linear output layer with a *rank bottleneck*. Such bottlenecked layers limit model expressivity. We investigate both theoretically and empirically how rank bottlenecks affect KGC models. We find that, by limiting the set of feasible predictions, rank bottlenecks hurt ranking accuracy and the distribution fidelity of scores. Inspired by the language modelling literature, we propose KGE-MoS, a mixture-based output layer to break rank bottlenecks in many KGC models. Our experiments on four datasets show that KGE-MoS improves performance and probabilistic fit of KGC models for a low parameter cost.

1 Introduction

Knowledge Graph Completion (KGC) aims to predict missing triples in a Knowledge Graph (KG) to improve its utility. For example, finding missing connections in a biomedical KG can reveal potential drug-disease associations [1, 2, 3], whereas in social networks or e-commerce, KGC models can be used as recommendation systems [4]. A common approach is to learn low-dimensional Knowledge Graph Embeddings (KGEs) for entities and relations and use them to score which entities are likely to be the object of a given subject-relation pair [5, 6].

The de facto standard KGE models for many applications multiply an embedding vector of the subject-relation query with the entity embedding matrix to score object entities. These models include bilinear and neural network approaches [7, 3, 8]. This vector-matrix multiplication linearly maps a hidden state of relatively low dimension (typically, 10^2 to 10^3) to a high-dimensional output space corresponding to the entities in the KG (typically, 10^4 to 10^6 for medium KGs, and up to 10^9 for industry-scale KGs [9]). Such linear output layers introduce low-rank constraints, often referred to as *rank bottlenecks*. Previous research showed that rank bottlenecks hurt Language Modelling (LM) perplexity [10], prompting non-linear augmentations as improvements [11, 12, 13]. Furthermore, rank bottlenecks also limit the set of feasible predictions in multilabel classifiers [14]. However, the impact of rank bottlenecks on KGC performance has not yet been explicitly studied, even though the order of magnitude between embedding dimensionality and number of entities in KGC can largely exceed the one between embedding dimensionality and vocabulary size in LM.

---

[*]Equal supervision contribution.
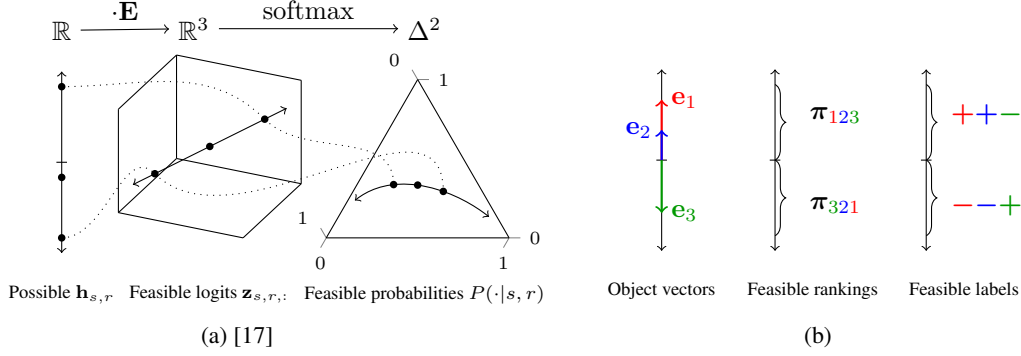 Code available at github.com/sonyresearch/kgemos

Figure 1: **Rank bottlenecks leave many score / ranking / sign-label reconstructions unfeasible** when $d < |\mathcal{E}| - 1$ (toy KGE, $d = 1$, $|\mathcal{E}| = 3$). (a) Projection of the hidden space of queries $(s, r, ?)$ by the matrix of object vectors $\mathbf{E}$. Logits lie in a 1D linear subspace. Probabilities after softmax lie in a 1D smooth manifold of the probability simplex, leaving all other points unfeasible. See Section 3.1. (b) Division of the hidden state space by object vectors $\mathbf{e}_o$ into regions corresponding to different rankings / labels. Many configurations (e.g., $\boldsymbol{\pi}_{132}$ or $+-+$) are unfeasible. See Section 3.2 and 3.3.

We show that a KGE model with a bottlenecked output layer can only predict a subset of the possible completions for a given query (see Figure 1). The standard prediction method ranks objects according to their scores. Alternatively, we can use scores to parameterise a multilabel classifier, with as many labels as the number of entities. We find that the rank bottleneck impacts both methods of prediction. Leveraging the graph factorisation literature, we establish a theoretical upper-bound on the necessary rank required for exact KG factorisation. We find this bound grows for larger and denser graphs. Finally, we can also use KGE scores to parameterise probabilistic predictors and enable downstream reasoning [15, 16]. Akin to perplexity in LM, we show that rank bottlenecks also severely limit the space of feasible probabilistic predictions of the KGC model.

To address rank bottlenecks in KGC, we propose to use a Mixture of Softmaxes (MoS) output layer for KGEs. MoS layers are a non-linear augmentation developed for LMs to break the rank bottleneck [10]. We derive KGE-MoS, a new output layer for KGEs to break their bottlenecks. We evaluate KGE-MoS on three KGE models across four knowledge graphs of increasing size and show that KGE-MoS improves both the ranking accuracy and probabilistic fit of probabilistic predictions, at a lower parameter cost than simply increasing the KGE dimension.

Contributions. In Section 3, we (i) highlight the implications of rank bottlenecks for reconstructing distributions (Section 3.1), for ranking predictions (Section 3.2) and for multilabel predictions (Section 3.3). In Section 4, we (ii) provide a theoretical bound for acceptable rank bottlenecks for ranking and multilabel predictions, depending on the graph connectivity. In Section 5, we (iii) introduce KGE-MoS, a simple solution to break rank bottlenecks. Our experimental results show that breaking rank bottlenecks improves ranking accuracy and particularly probabilistic fit for a low parameter cost.

2 Knowledge Graph Completion

A Knowledge Graph (KG) is a common data structure for representing information. We study the Knowledge Graph Completion (KGC) task, where the goal is to predict information missing from a given KG. Let $\mathcal{E}$ be a set of entities and $\mathcal{R}$ a set of relations. A KG $\mathcal{G} = \{(s, r, o) \in \mathcal{E} \times \mathcal{R} \times \mathcal{E}\}$ is a set of triples where $s \in \mathcal{E}$ is a subject, $r \in \mathcal{R}$ is a relation, and $o \in \mathcal{E}$ is an object.[1] In the KGC task, only some triples $\mathcal{G}_{obs} \subset \mathcal{G}$ are observed, and the task is to predict missing triples $\mathcal{G} \setminus \mathcal{G}_{obs}$ by predicting suitable objects for $(s, r, ?)$ queries. This is typically cast as a ranking problem where candidate objects are evaluated and ranked; correct answers are the objects o such that $(s, r, o) \in \mathcal{G}$ [5, 7, 8].

A Knowledge Graph Embedding model (KGE) is a function $\phi : \mathcal{E} \times \mathcal{R} \times \mathcal{E} \to \mathbb{R}$ that assigns a score $z_{s,r,o}$ to each triple by embedding entities and relations. Here, higher scores correspond to more

---

[1] We use a, $\mathbf{a}$, $\mathbf{A}$, $\mathcal{A}$ to denote scalars, vectors, matrices, and tensors respectively. Indexing and slicing follows the usual convention, see [18] or Appendix A for details.

likely triples. We use $\mathbf{e}_s, \mathbf{e}_o \in \mathbb{R}^d$ to denote the embeddings of subject and object entities respectively and $\mathbf{w}_r \in \mathbb{R}^{d_r}$ to denote the embedding of a relation r (often, $d_r = d$). Let $\mathcal{Z} \in \mathbb{R}^{|\mathcal{E}| \times |\mathcal{R}| \times |\mathcal{E}|}$ be the scores calculated for each triple arranged in a tensor. A KGE answers object prediction queries $(s, r, ?)$ by ordering entities by decreasing values of $\mathbf{z}_{s,r,:} \in \mathbb{R}^{|\mathcal{E}|}$.

2.1 Object prediction as a vector-matrix multiplication

In this work, we focus on KGEs of the form

$$\phi(s, r, o) = \mathbf{h}_{s,r}^\top \mathbf{e}_o. \tag{1}$$

Here $\mathbf{h}_{s,r} \in \mathbb{R}^d$ is a representation of the subject and relation, and is typically the result of an encoding function $h(\mathbf{e}_s, \mathbf{w}_r)$. KGEs then use a simple dot product with the object embedding $\mathbf{e}_o$ to compute a score, which enables fast scoring for object prediction. Indeed, let $\mathbf{E} \in \mathbb{R}^{|\mathcal{E}| \times d}$ be the embeddings of all entities stacked in a matrix. The computation of scores for a fixed subject-relation pair (s, r) against all entities o becomes the efficient vector-matrix multiplication

$$\mathbf{z}_{s,r,:} = \mathbf{h}_{s,r} \mathbf{E}^\top. \tag{2}$$

Bilinear models use score functions linear in the subject and object embeddings, the latter recovering eq. (1). In RESCAL's score function $\mathbf{e}_s^\top \mathbf{W}_r \mathbf{e}_o$ [19], we have $\mathbf{h}_{s,r}^\top = \mathbf{e}_s^\top \mathbf{W}_r$, where $\mathbf{W}_r \in \mathbb{R}^{d \times d}$ is a matrix of shared parameters for relation r. In the score function $(\mathbf{e}_s \odot \mathbf{w}_r)^\top \mathbf{e}_o$ of DISTMULT [20], we have $\mathbf{h}_{s,r}^\top = (\mathbf{e}_s \odot \mathbf{w}_r)^\top$, where $\odot$ is the element-wise (Hadamard) product, and $\mathbf{e}_s, \mathbf{w}_r, \mathbf{e}_o \in \mathbb{R}^d$. The same can be derived for COMPLEX [21], an extension of DISTMULT to complex-valued embeddings to handle asymmetry in the score function, or for CP [22] and SIMPLE [23], which use different embedding spaces for subjects and objects. In fact, eq. (1) holds for TUCKER [24], a model that generalises all the above bilinear models as tensor decompositions. We detail how to rewrite each of these models as $\mathbf{h}_{s,r}^\top \mathbf{e}_o$ in Appendix D.1.

We can also interpret *neural network models* for KGC under the perspective of eq. (1). Neural KGEs use neural networks to encode the subject and relation into a hidden state $\mathbf{h}_{s,r} = \text{NeuralNet}(\mathbf{e}_s, \mathbf{w}_r)$. Therefore, they are an expressive alternative for modelling non-linear interactions between entities and relations. The hidden state is then projected to logits in the object space using a linear (or affine) layer. This gives a score function of the form $\mathbf{h}_{s,r}^\top \mathbf{e}_o$ (up to a bias term, in the case of an affine layer). Neural KGEs that embed subject and objects before linearly combining them use, for example, 2D CNNs in CONVE [25], 1D CNNs in HYPERE [26], transformers in STARE [27], and graph convolutional networks in R-GCNS [28].

2.2 Output functions and task objectives

The introduction of new KGEs over the years went along with the introduction of new approaches for training them. Early KGEs ranked true triples higher using margin-based loss [29, 20], while later models shifted towards multi-label classification with binary cross-entropy (BCE) [21, 25, 30] or parameterised softmax layers with cross-entropy (CE) to model object distributions given a subject and relation [31, 32, 33]. For a detailed overview, see Appendix D.2 and related surveys [7, 8]. While KGEs are generally evaluated on ranking metrics, the choice of the output and corresponding loss functions often reflects different underlying task objectives. We introduce three such underlying tasks of increasing difficulty.

Ranking reconstruction (RR) Given a query of the form $(s, r, ?)$, ranking reconstruction aims to assign scores such that each true target object o receives a higher score $z_{s,r,o}$ than any non-target object o', i.e., $z_{s,r,o} > z_{s,r,o'}$ for all o and o' with $(s, r, o) \in \mathcal{G}$ and $(s, r, o') \notin \mathcal{G}$.

Sign reconstruction (SR) For a query $(s, r, ?)$, sign reconstruction aims to learn a scoring function such that $z_{s,r,o} > 0$ if $(s, r, o) \in \mathcal{G}$, and $z_{s,r,o} < 0$ otherwise. This objective can be viewed as binary classification over triples.

Distributional reconstruction (DR) Given a query $(s, r, ?)$, distributional reconstruction aims to recover uniform scores $z_{s,r,o} = \tau_+$ for all $(s, r, o) \in \mathcal{G}$ and $z_{s,r,o'} = \tau_-$ for all $(s, r, o') \notin \mathcal{G}$, with τ_+ a high score for true triples and $\tau_- < \tau_+$ a low score for negative triples. For example, $\tau_+ = 1$ and $\tau_- = 0$ corresponds to exact binary reconstruction. Other examples

can be under probabilistic interpretations, e.g., $\tau_- \approx -\infty$ for softmax layers and τ_+ to define a uniform probability distribution for the true scores. Such exact reconstruction can be used for downstream reasoning. For example, [15, 16] combine binary prediction scores of simple queries to answer complex queries, which demands well-distributed simple scores. Another example is to use scores for sampling [33] which demands accurate data distributions.

We will say that a KGE is *expressive* for a task under a certain condition (typically, a dimensionality bound on its parameters) if there exists a parameter setting that satisfies the task objective under that condition. Notice that any model expressive for DR or SR is also expressive for RR. Moreover, by setting a decision threshold (e.g., $\frac{\tau_+ + \tau_-}{2}$), we can repurpose a model for DR to a model for SR.

Several KGEs are fully expressive, but the underlying theoretical conditions are impractical for real-world datasets. For example, TUCKER is fully expressive for any graph when the embedding dimensions satisfy $d_e = |\mathcal{E}|$ and $d_r = |\mathcal{R}|$ [24], and COMPLEX achieves full expressivity with $d_e = d_r = |\mathcal{E}||\mathcal{R}|$ [21]. Such requirements are unrealistic for larger datasets (e.g., $|\mathcal{E}| = 10^6$), making these theoretical guarantees not applicable in practice: typically, $d \ll |\mathcal{E}|$ by several orders of magnitude. This severely limits the expressivity of KGEs, as we discuss next.

3 Rank Bottlenecks in KGEs...

In this section, we discuss the practical limitations in expressivity of bottlenecked KGEs in relation to each task objective defined above. We define a *bottlenecked KGE* as a KGE model that uses a vector-matrix multiplication for object prediction (see Section 2.1) and that has a dimension $d < |\mathcal{E}| - 1$. As the entity embedding matrix $\mathbf{E}$ has rank at-most d, the score vector $\mathbf{z}_{s,r,:}$ is confined to a d-dimensional linear subspace of $\mathbb{R}^{|\mathcal{E}|}$. For a visual intuition, consider the bottlenecked KGE depicted in Figure 1a with $d = 1$ and $|\mathcal{E}| = 3$.

Bottlenecks are typically not an issue for intermediate layers in a neural network because repeated non-linear transformations can reshape the linear subspace to meaningful non-linear manifolds (e.g., as seen in autoencoders [34]). In fact, it can help with computational efficiency and with generalisation if we assume that the data lies approximately on a low-dimensional manifold [35]. However, a bottleneck at the output layer of a model imposes more rigid limitations. We discuss each in the context of the task objectives introduced in Section 2.2, focusing first on scores for a distributional reconstruction of the KG, then for a ranking reconstruction of the KG, and finally for a sign reconstruction of the KG.

3.1 ... for solving distributional reconstruction

Rank bottlenecks limit the predictive capability of a KGE, which can be demonstrated by comparing the rank of the knowledge graph's adjacency matrix to that of the KGE score matrix. Consider $\mathbf{Z} = \begin{bmatrix} \mathbf{z}_{1,1,:} \\ \vdots \\ \mathbf{z}_{|\mathcal{E}|,|\mathcal{R}|,:} \end{bmatrix} \in \mathbb{R}^{|\mathcal{E}||\mathcal{R}| \times |\mathcal{E}|}$, a view of the score tensor $\mathcal{Z}$ rearranged to have subject-relation pairs on the first axis and objects on the second. [2] As $\mathbf{Z} = \mathbf{H}\mathbf{E}^\top$, where $\mathbf{H} = \begin{bmatrix} \mathbf{h}_{1,1} \\ \vdots \\ \mathbf{h}_{|\mathcal{E}|,|\mathcal{R}|} \end{bmatrix} \in \mathbb{R}^{|\mathcal{E}||\mathcal{R}| \times d}$ is the matrix of hidden states for each subject-relation pair, the rank of $\mathbf{Z}$ is at most d. Consider now the ground truth adjacency matrix of the graph $\mathbf{Y} \in \{0,1\}^{|\mathcal{E}||\mathcal{R}| \times |\mathcal{E}|}$, where $y_{i,o}$ is one if o is an object for the subject-relation pair i and 0 otherwise. If $\mathbf{Y}$ has a rank r greater than d, it means that the ground truth relationships lie in a higher-dimensional space than the d-dimensional subspace spanned by the KGE scores. This leads to a trivial limitation in the model's ability to accurately represent the true relationships.

Proposition 3.1 (DR bottleneck)**.** *A bottlenecked KGE constrained to a low-rank d cannot perfectly represent the distributions in a true adjacency matrix $\mathbf{Y} \in \{0,1\}^{|\mathcal{E}||\mathcal{R}| \times |\mathcal{E}|}$ with rank $r > d + 1$.*

Proof. Consider a perfect solution $\mathbf{Z}^\star$ for DR as introduced in 2.2, which assigns a uniform high score τ_+ to true triples and a uniform low score τ_- to false ones. The solution should satisfy

---

[2]Formally, this would be the transposed mode-3 unfolding $\mathbf{Z}_{(3)}^\top$ of $\mathcal{Z}$, but we will denote it $\mathbf{Z}$ for simplicity.

$\mathbf{Y} = \frac{1}{\tau_+}(\mathbf{Z}^\star - \tau_- \mathbf{1})$, where $\mathbf{1}$ is a matrix of ones with the same size as $\mathbf{Y}$. Since $\mathbf{Z}^\star$ has rank at most d and $\tau_- \mathbf{1}$ is a matrix of rank at most 1, the equality is impossible if $\mathbf{Y}$ has rank $r > d + 1$. $\qquad\square$

Notice that applying a softmax function on the scores, despite introducing non-linear interactions, still limits the feasible predictions in a rigid way. Softmax maps the d-dimensional linear subspace of scores to a smooth d-dimensional manifold within the corresponding probability simplex $\Delta^{|\mathcal{E}|-1}$ (see Figure 1a) [17]. However, because softmax is log-linear, the manifold is rigidly constrained to certain shapes. Intuitively, this implies that class probability ratios on the manifold are linear on a logarithmic scale. Any groundtruth that does not adhere to this constraint cannot be represented. We discuss this phenomenon called *softmax bottleneck* [10] in more detail in Appendix E.1.

3.2 ... for solving ranking reconstruction

Next, we discuss how rank bottlenecks affect a model's ability to correctly order potential objects, which is crucial for the usual KGC evaluation protocols. Borrowing the notation of [36], let $\boldsymbol{\pi}$ denote a permutation of objects. For example, in Figure 1b, the scores $\mathbf{z}_{s,r,:} = \mathbf{h}_{s,r}\mathbf{E}^\top = [-2 \quad -0.5 \quad 3.]$ would imply that we assign the query $\mathbf{h}_{s,r}$ the ranking $\boldsymbol{\pi}_{321}$ since $z_{s,r,3} > z_{s,r,2} > z_{s,r,1}$. Notice that activations like sigmoid of softmax preserve the ranking.

Theorem 3.2 (RR bottleneck). *A bottlenecked KGE with low-rank $d < |\mathcal{E}| - 1$ always has some unfeasible ranking configurations $\boldsymbol{\pi}$, regardless of the learned input representations.*

Proof. We use the result from [37, 38, 36] which states that a linear (affine) classifier over N classes parameterised by a weight matrix $\mathbf{W} \in \mathbb{R}^{N \times d}$ (and bias vector $\mathbf{b} \in \mathbb{R}^N$) followed by any monotonic activation, can only predict a subset of class rankings if $d < N - 1$. Replacing $\mathbf{W} \in \mathbb{R}^{N \times d}$ with $\mathbf{E} \in \mathbb{R}^{|\mathcal{E}| \times d}$ yields the theorem. Additionally, for object vectors in general position, if we fix d, changing $\mathbf{E}$ changes the set of rankings that are feasible, but not the cardinality of the set. The cardinality can be calculated using Stirling numbers with a proof that stems from finding the maximum and generic number of distance-based orderings of N points in a d-dimensional space [37, 38, 39]. The narrower the low-rank d, the more class permutations $\boldsymbol{\pi}$ become infeasible. $\qquad\square$

For example, in Figure 1b (our $d = 1, |\mathcal{E}| = 3$ toy model), we see that only the rankings $\boldsymbol{\pi}_{123}$ and $\boldsymbol{\pi}_{321}$ are feasible. If one query i has a different ground truth ranking (e.g., $\boldsymbol{\pi}_{213}$), then even the most powerful encoder for $\mathbf{h}_{s,r}$ cannot achieve the ground truth ranking.

3.3 ... for solving sign reconstruction

We obtain a similar result for the SR task. Let $\mathbf{y} \in \{+, -\}^{|\mathcal{E}|}$ be the multi-label assignment of a query. For example, in Figure 1b, if we obtain the scores $\mathbf{z}_{s,r,:} = \mathbf{h}_{s,r}\mathbf{E}^\top = [-2 \quad -0.5 \quad 3.]$, we assign the query $\mathbf{h}_i$ the multi-label assignment $\mathbf{y} = [- \quad - \quad +]$.

Theorem 3.3 (SR bottleneck). *A bottlenecked KGE with low-rank $d < |\mathcal{E}|$ always has some unfeasible multi-label assignments configurations $\mathbf{y}$, regardless of the learned input representations.*

Proof. We use the result from [40, 14] which states that a linear (affine) classifier over N classes parameterised by a low-rank weight matrix $\mathbf{W} \in \mathbb{R}^{N \times d}$ (and bias vector $\mathbf{b} \in \mathbb{R}^N$) can only predict a subset of multi-label assignments configurations $\mathbf{y}$ if $d < N$ using the decision rule $\text{sign}(\mathbf{Wx} + \mathbf{b})$ for input $\mathbf{x} \in \mathbb{R}^d$. Replacing $\mathbf{W} \in \mathbb{R}^{N \times d}$ with $\mathbf{E} \in \mathbb{R}^{|\mathcal{E}| \times d}$ yields the theorem. For a linear layer, the number of feasible assignments is upper-bounded by $2\sum_{i=0}^{d-1}\binom{N-1}{i}$. For an affine layer, more assignments are feasible, but the increase in the number of feasible assignments is less than what would be achieved by increasing the embedding dimension d by one. $\qquad\square$

For example, in Figure 1b, we see that only the multi-label assignments $++-$ and $--+$ are feasible. For any assignment $\mathbf{y}_j$ that is different from these two, it is impossible to learn a representation $\mathbf{h}_j$ such that the KGE classifies it correctly.

Table 1: Sufficient embedding dimension d_{SR}^+ for exact sign reconstruction of $(s, r, ?)$ queries on different KGs, including inverse relations. The dimension scales with the maximum graph out-degree c^+ rather than simply the number of entities. See Theorem 4.1.

Dataset	#Entities	#Rels	Average out-degree	d_{SR}^+
FB15k-237	14,541	237	3.83	8,729
Hetionet	45,158	24	21.66	30,073
ogbl-biokg	93,773	51	37.48	58,657
openbiolink	180,992	28	18.12	36,841

4 A sufficient bound for sign and ranking reconstruction

While our theoretical results prove that bottlenecked KGEs cannot reconstruct some ranking and sign predictions, an important question remains: is there a bottlenecked model which, while unable to represent all possible results, can accurately represent the groundtruth ones relevant to the Knowledge Graph? We address this by leveraging the graph's structure to derive an upper bound on an embedding dimension d that is sufficient for accurate sign reconstruction.

Theorem 4.1. *Let* $\mathbf{Y} \in \{0, 1\}^{|\mathcal{E}||\mathcal{R}| \times |\mathcal{E}|}$ *be the representation of the KG with subject-relation pairs on the first axis and objects on the second. Let the sign function* $s(x) = 1$ *if* $x > 0$ *and* $s(x) = 0$ *otherwise. Then,* $\mathbf{Y}$ *can be exactly decomposed as* $\mathbf{Y} = s(\mathbf{H}\mathbf{E}^\top)$ *where* $\mathbf{H} \in \mathbb{R}^{|\mathcal{E}||\mathcal{R}| \times (2c^+ + 1)}$, $\mathbf{E} \in \mathbb{R}^{|\mathcal{E}| \times (2c^+ + 1)}$, *and* c^+ *is the maximum out-degree across all subject-relation pairs in the KG. The function* $s(\cdot)$ *is applied element-wise.*

Proof. The proof extends the reasoning of Theorem 6 of [41] for bounding the sign rank of sparse matrices to rectangular bipartite matrices and is detailed in Appendix B. □

Corollary 4.2 (Sufficient rank for sign and ranking reconstruction). *For any KG with maximum out-degree* c^+ *across subject-relation pairs, there exists a KGE with rank* $d_{SR}^+ = 2c^+ + 1$ *that achieves perfect sign reconstruction for queries* $(s, r, ?)$. *By extension, the KGE also achieves perfect ranking reconstruction, as positive scores for existing facts rank above negative scores for non-existing facts.*

Table 1 presents the theoretical sufficient dimension $d_{\text{SR}}^+ = 2c^+ + 1$ for several KGs. These results demonstrate that the required dimension can be significantly lower than the total number of entities in the graph. Crucially, the bound is determined by the graph's maximum subject-relation out-degree c^+, reflecting its connectivity, rather than simply the number of nodes. This explains why a dataset like `ogbl-biokg`, despite having fewer nodes than `openbiolink`, requires a higher theoretical dimension due to its greater connectivity (implied by its higher average out-degree in the table).

While $2c^+ + 1$ serves as a general upper bound, for KGs with specific structural properties like power-law degree distributions, tighter bounds may be possible (see Fig. 3 in appendix).

However, two practical questions remain. First, can existing KGEs, with their specific scoring functions, actually represent the factorisation described in Theorem 4.1? Second, even if they can, can this solution be efficiently learned through gradient-based optimisation in practice? Despite these challenges, this theoretical result provides a valuable guide for dimensionality choices.

5 Breaking rank bottlenecks with a mixture of softmaxes

Having shown how rank bottlenecks limit the feasible predictions of KGEs, we now propose a solution to break these rank bottlenecks. A simple approach is to use a larger embedding dimension d to reflect the graph size or, according to the bound of Theorem 4, its connectivity. However, this quickly becomes impractical for large graphs. Instead, we adapt the *Mixture of Softmaxes* (MoS) solution, originally proposed in language modelling [10], to KGEs.

Let O be a random variable over the objects. Softmax is used with KGE models for object prediction $(s, r, ?)$ to model a categorical distribution $P(O|s, r) = \text{softmax}(\mathbf{h}_{s,r}\mathbf{E}^\top) \in \Delta^{|\mathcal{E}|-1}$, where $\Delta^{|\mathcal{E}|-1}$ is the probability simplex over the objects. This distribution should align with the data distribution (labels of the corresponding triples, normalised to sum to 1). Although softmax is traditionally used for predicting a single correct class, it is repurposed in KGC for multi-label scenarios by retrieving top-k entries, ranking likely completions (RR) and modelling well-distributed scores (DR, e.g. for

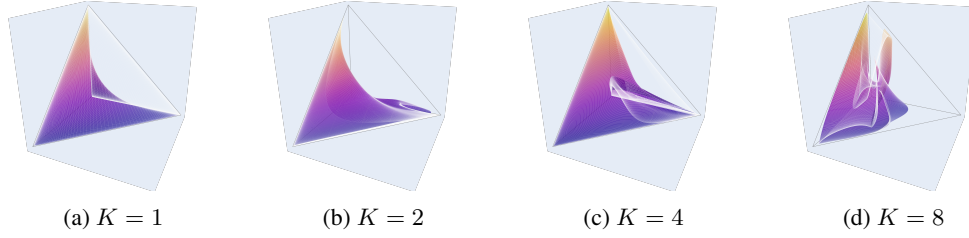| (a) $K = 1$ | (b) $K = 2$ | (c) $K = 4$ | (d) $K = 8$ |

Figure 2: Feasible distributions of randomly initialised KGE-MoS layers ($d = 2, |\mathcal{E}| = 4$). The points are calculated for different inputs $\mathbf{h}_{s,r}$ while $\mathbf{E}$, $\boldsymbol{\omega}_k$ and $f_{\boldsymbol{\theta}_k}$ are fixed. A higher number of softmaxes K has a higher representational power and can better fit arbitrary ground truths $P^*(O|s,r)$.

sampling [33]). Extensive benchmarking efforts have shown that training KGEs with softmax and CE loss leads to the best results [7, 8].

As shown in Sections 3.1 and 3.2, a bottlenecked KGE model with a softmax activation cannot represent all possible distributions and rankings over the objects. We propose to use a KGE-MoS layer, which is a mixture of K softmaxes, to break these rank bottlenecks. Specifically,

$$P(O|s,r) = \sum_{k=1}^{K} \pi_{s,r,k} \operatorname{softmax}(f_{\boldsymbol{\theta}_k}(\mathbf{h}_{s,r})\mathbf{E}^\top), \quad \sum_{k=1}^{K} \pi_{s,r,k} = 1, \tag{3}$$

where $\pi_{s,r,k} \in [0,1]$ is the prior or mixture weight of the k-th component and $f_{\boldsymbol{\theta}_k}(\mathbf{h}_{s,r}) \in \mathbb{R}^d$ is the k-th context vector associated with the input (s,r). The prior is parameterised as $\pi_{s,r,k} = \exp \mathbf{h}_{s,r}^\top \boldsymbol{\omega}_k / \sum_{k'} \exp \mathbf{h}_{s,r}^\top \boldsymbol{\omega}_{k'}$ with $\boldsymbol{\omega}_k \in \mathbb{R}^d$. The context vector $f_{\boldsymbol{\theta}_k}(\mathbf{h}_{s,r})$ is obtained by mapping the hidden state with a component-specific projection $f_{\boldsymbol{\theta}_k}$. $\boldsymbol{\theta}_k$ and $\boldsymbol{\omega}_k$ are component-specific parameters. In this work, we model each $f_{\boldsymbol{\theta}_k}$ with a two-layer network.

The weighted combinations of softmaxes is a non-linear transformation of logits which, while not increasing the dimension of the subspace spanned by the KGE, allows for a more complex set of distributions to be represented (see Figure 2). A more algebraic perspective is to consider the empirical log-probability matrix of the KGE predictions (see Appendix E.1), which resides in a linear subspace with $K = 1$ softmax and in a non-linear subspace when $K > 1$ [10].

KGE-MoS is a drop-in solution that can be applied to any KGE method presented in Section 2.1 (e.g., CONVE). Simply replacing their output layer results in a high-rank variant (e.g., CONVE-MoS) for a low parameter cost $O(Kd + K|\boldsymbol{\theta}_k|)$, which in our case gives $O(Kd^2)$. In contrast, increasing the dimension of the KGE by a factor d_{inc} has a cost $O(d_{\text{inc}}(|\mathcal{E}| + |\mathcal{R}|))$ which is usually less scalable as $|\mathcal{E}| \gg Kd$. Notice that while bilinear models (e.g., DISTMULT) can perform subject prediction $(?, r, o)$ scalably as a vector-matrix multiplication, their augmentations (e.g., DISTMULT-MoS) cannot, and must rely on inverse relations $(o, r^{-1}, ?)$. We discuss this in Appendix C.

6   Experiments

We aim to answer the following research questions: **(RQ1)** "How does the performance of models equipped with the proposed KGE-MoS output layer compare to that of bottlenecked KGE models?" **(RQ2)** "How does the performance of increasing the embedding size of a KGE compare to the proposed KGE-MoS output layer?"

Datasets   We evaluate the performance of KGE models on the following standard datasets for link prediction: FB15k-237 [42], Hetionet [1], ogbl-biokg [4], and openbiolink [2]. FB15k-237 is a commonly used KGC benchmark, but its size ($|\mathcal{E}| \approx 10^4$) is relatively small compared to modern KGs. We choose the other datasets for their larger sizes ($|\mathcal{E}| \approx 10^5, 10^6$), as we expect rank bottlenecks to be more impactful in larger graphs. See Appendix F.1 for details and statistics.

Models   For the baseline KGE models, we use DISTMULT [20], RESCAL [20], and CONVE [25], each trained using a softmax output layer and inverse relations for subject prediction, as they are

standard choices for link prediction [7, 8]. We use the best performing hyperparameters found for each model in previous works [7] (see Appendix F.3). We compare the baselines with their high-rank variants DISTMULT-MOS, RESCAL-MOS, and CONVE-MOS, where we replace the standard softmax layer with our proposed mixture of $K = 4$ softmaxes (Section 5). We train each model with embedding dimensions $d = 200$ and $d = 1000$. The hyperparameters of the KGE-MOS output layer are obtained using a simple random search on the `ogbl-biokg` dataset and detailed in Appendix F.3.

Metrics As usual [5, 7, 8], we assess the models for predicting object queries $(s, r, ?)$ and subject queries $(?, r, o)$ using filtered mean reciprocal rank (MRR) (see Appendix F.2). We measure the distributional fidelity of the models using the Negative Log Likelihood (NLL) of the model predictions on the test set. Whereas previous work [33] directly reports the NLL, we introduce a *filtered NLL* metric which more accurately reflects the predictive performance of a model for KGC. When evaluating the NLL on the test set, given a $(s, r, ?)$ query, we zero out the probabilities of ground truth objects for that query seen during training, renormalising the probabilities of the model predictions. Formally, given a model prediction $P(o|s, r)$, we define the filtered test probability as

$$P^{\text{filtered}}(o|s, r) = \frac{\mathbb{1}[(s, r, o) \notin \mathcal{G}_{\text{train}}]P(o|s, r)}{\sum_{o' \in \mathcal{E}} \mathbb{1}[(s, r, o') \notin \mathcal{G}_{\text{train}}]P(o'|s, r)} \tag{4}$$

Because in KGC training and test sets are disjoint, the filtered NLL prevents the penalisation of trained models that leave less probability mass for test triples, but that are capable of distinguishing test triples from truly negative triples. This is discussed in detail in Appendix F.2.

6.1 Results

Our results are reported in Table 2. Each of the twelve models (six models $\times$ two embedding sizes) is run three times per dataset with different initialisations for statistical significance.

(RQ1) On the three larger datasets, the best performing models are consistently KGE-MOS models. The best performing model is often DISTMULT-MOS, hinting that a simple encoder for the subject-relation with an elaborate output layer for the objects might be the most effective approach. In contrast, on the smallest dataset `FB15k-237`, KGE-MOS does not show an improvement over the bottlenecked KGE models. In fact, the best KGE at $d = 200$ (CONVE) performs almost equally to the best KGE at $d = 1000$ (DISTMULT), hinting that rank bottlenecks are not critical at this dataset scale.

(RQ2) On the three larger datasets, KGE-MOS at $d = 200$ obtains almost as strong performance as the bottlenecked baselines at $d = 1000$. Still, the performance increase of KGE-MOS models is larger at $d = 1000$ than at $d = 200$, suggesting that increasing embedding dimension not only helps with bottlenecks, it also unlocks input representation power.

Mixture ablation Next, we run an ablation on the number of softmaxes used in KGE-MOS. We use `ogbl-biokg`, as Section 4 suggests it to be the most challenging dataset for bottlenecks due to its high connectivity, and DISTMULT-MOS, the best performing model. Table 3 details the results, with each value averaged over three runs. Increasing the number of softmaxes consistently leads to better performance, which is explainable by the larger representational power at each level (Figure 2). Notice that DISTMULT-MOS at $K = 1$, which does not mix any softmaxes and is a bottlenecked baseline, outperforms DISTMULT. This result can only be due to the projection layer f_{θ_k}. DISTMULT is known to be incapable of representing asymmetric relations ($\phi(s, r, o) = \phi(o, r, s)$ in DISTMULT) [21, 22]. The projection layer adds asymmetry, which solves the limitation and likely explains the improvement.

Computational cost While KGE-MOS has a marginal parameter cost, its computational cost is higher than that of a regular softmax layer. On `openbiolink`, the dataset with the largest output layer, we find that KGE-MOS at $K = 4$ is between 1.69 and 2.75 times slower than its bottlenecked baseline for a training step. The largest difference is recorded for DISTMULT and DISTMULT-MOS, given that DISTMULT is a very simple model. Still, we notice that the number of softmaxes has a negligible impact on inference time. See Table 10 for details. We find most of the overhead is due to the computation of the projections $f_{\theta_k}(\mathbf{h}_{s,r})$. Therefore, if inference time is a concern, this can be mitigated by using a more simple, efficient projection layer.

Table 2: **KGE-MoS improves performance and probabilistic fit of KGE models.** Average NLL ↓ and MRR ↑ for datasets of increasing sizes. Standard deviations and other ranking metrics are reported in Appendix F.4. Best results per dataset and dimension in **bold**. We also report the average improvement in NLL and MRR (mixture vs regular) per dataset and dimension. ⋆ indicates statistical significance at $p < 0.05$ in a Wilcoxon signed-rank test pairing each model with its mixture variant.

MODEL	FB15k-237			HETIONET			ogbl-biokg			OPENBIOLINK		
	NLL	MRR	PARAM	NLL	MRR	PARAM	NLL	MRR	PARAM	NLL	MRR	PARAM
d = 200												
DISTMULT	4.74	.304	3.0M	6.10	.250	9.0M	4.83	.792	18.8M	5.14	.302	36.2M
DISTMULT-MOS	4.65	.306	3.3M	**5.83**	**.277**	9.4M	**4.65**	**.792**	19.1M	5.03	.314	36.5M
RESCAL	4.79	.258	21.9M	6.13	.219	10.9M	4.89	.763	22.8M	5.16	.303	38.4M
RESCAL-MOS	4.65	.318	22.2M	5.87	.274	11.3M	4.70	.780	23.2M	**5.04**	**.323**	38.8M
CONVE	**4.48**	**.321**	5.1M	6.03	.252	11.1M	4.94	.782	20.8M	5.28	.286	38.3M
CONVE-MOS	4.57	.311	5.4M	5.92	.263	11.4M	4.77	.768	21.2M	5.10	.304	38.6M
avg -MoS delta	-.05	.009		*-.22	*.031		*-.18	.000		*-.14	*.017	
d = 1000												
DISTMULT	**4.56**	**.331**	15.0M	6.04	.288	45.2M	4.89	.801	93.9M	5.17	.316	181.0M
DISTMULT-MOS	4.72	.311	23.0M	5.76	.312	53.2M	**4.34**	**.837**	101.9M	**4.89**	**.347**	189.0M
RESCAL	4.64	.307	488.5M	5.93	.243	93.1M	4.74	.799	195.8M	5.03	.328	237.0M
RESCAL-MOS	4.63	.325	496.5M	5.87	.300	101.2M	4.42	.824	203.8M	5.00	.328	245.0M
CONVE	4.65	.301	70.1M	6.06	.262	100.3M	4.93	.807	149.0M	5.24	.308	236.2M
CONVE-MOS	4.69	.316	78.2M	**5.71**	**.313**	108.3M	4.43	.817	157.0M	4.91	.336	244.2M
avg -MoS delta	.06	.004		*-.23	*.044		*-.45	*.022		*-.19	*.018	

Table 3: MRR and NLL on `ogbl-biokg` at $d = 1000$ with different numbers of softmaxes.

MODEL	#SOFTMAXES	NLL ↓	MRR ↑
DISTMULT	1	4.89±0.02	.801±.002
DISTMULT-MOS	1	4.42±0.01	.821±.000
DISTMULT-MOS	2	4.37±0.01	.831±.001
DISTMULT-MOS	4	4.34±0.01	.837±.001
DISTMULT-MOS	8	**4.33±0.00**	**.841±.001**

7 Related work

Rank bottlenecks Rank bottlenecks in output layers of neural networks were first studied in *softmax models* for language modelling [10]. If the task is to predict a single best completion for a query, low-rank constraints are less problematic [36]. However, to predict a distribution over the vocabulary or all plausible completions of a prompt, rank bottlenecks severely limit the expressivity of the model. [10] proposed a mixture of softmaxes as an output layer to break the rank bottleneck in language modelling. [11] proposed a variant, more scalable mixture model, whereas [12, 13] proposed alternative non-linearities. [14] explored rank bottlenecks in clinical and image *multi-label classification* and proposed a discrete Fourier transform output layer to guarantee a minimum number of label combinations to be feasible. To the best of our knowledge, we are the first to study rank bottlenecks in the context of KGC. Earlier works [21, 23, 24] have given theoretical guarantees on the expressivity of KGE models, but the provided conditions on the embedding dimension (e.g., $d \geq |\mathcal{E}|$) are unrealistic for large datasets. Recent work [15, 16, 43, 44] has also emphasised the importance and lack of well-distributed output scores of KGE models for downstream reasoning.

Object prediction without vector-matrix multiplication Translation-based KGE models [29, 45, 46, 47] score objects using distance metrics like $\|\mathbf{h}_{s,r} - \mathbf{e}_o\|$, where relations act as geometric transformations (translations or rotations) in vector space. Translational models are interpretable and fast but are generally not fully expressive. Region-based models [48] replace vector translations with geometric containment. Entities are embedded as points and relations as boxes. Scoring is based on whether objects lie within the box defined by the subject and relation. Box embeddings prioritise spatial interpretability and complex inference patterns (e.g., hierarchical rule injection).

8 Conclusions

In this paper, we showed that rank bottlenecks are a fundamental limitation of many standard KGE models. We demonstrated how these bottlenecks limit the model's expressivity, affecting ranking accuracy and the distributional fidelity of probabilistic predictions. To address this, we introduced KGE-MoS, a mixture-based output layer that effectively breaks rank bottlenecks. Our experiments across four datasets show that KGE-MoS improves both performance and distributional fidelity of KGC models, at only a small increase in parameters. Our findings suggest that exploring other solutions for breaking rank bottlenecks is a promising avenue for advancing KGC.

Limitations Although our bound on a sufficient embedding dimension for sign and ranking reconstruction is a useful hint to decide a model dimension, it is not tight for all KGs and the solution used as a proof may not be representable by current KGE models. In practice, this means that a bottlenecked model may need more dimensions than suggested by the bound. Secondly, while we have shown that KGE-MoS improves performance by breaking the rank bottleneck, the computational cost during inference is higher than standard KGE models. This can be mitigated by using more efficient projection layers. Finally, we did not evaluate KGE-MoS on Knowledge Graphs with more than millions of entities. Exploring its performance and scalability in settings with significantly larger KGs remains an important avenue for future research.

Acknowledgements

References

[1] Daniel Scott Himmelstein, Antoine Lizee, Christine Hessler, Leo Brueggeman, Sabrina L Chen, Dexter Hadley, Ari Green, Pouya Khankhanian, and Sergio E Baranzini. Systematic integration of biomedical knowledge prioritizes drugs for repurposing. *eLife*, 6:e26726, September 2017.

[2] Anna Breit, Simon Ott, Asan Agibetov, and Matthias Samwald. OpenBioLink: a benchmarking framework for large-scale biomedical link prediction. *Bioinformatics*, 36(13):4097–4098, July 2020.

[3] Stephen Bonner, Ian P. Barrett, Cheng Ye, Rowan Swiers, Ola Engkvist, Charles Tapley Hoyt, and William L. Hamilton. Understanding the performance of knowledge graph embeddings in drug discovery. *Artificial Intelligence in the Life Sciences*, 2:100036, December 2022.

[4] Weihua Hu, Matthias Fey, Marinka Zitnik, Yuxiao Dong, Hongyu Ren, Bowen Liu, Michele Catasta, and Jure Leskovec. Open Graph Benchmark: Datasets for Machine Learning on Graphs, 2020. Version Number: 7.

[5] Maximilian Nickel, Kevin Murphy, Volker Tresp, and Evgeniy Gabrilovich. A Review of Relational Machine Learning for Knowledge Graphs. 2015. Publisher: arXiv Version Number: 3.

[6] Shaoxiong Ji, Shirui Pan, Erik Cambria, Pekka Marttinen, and Philip S. Yu. A Survey on Knowledge Graphs: Representation, Acquisition and Applications. *IEEE Transactions on Neural Networks and Learning Systems*, 33(2):494–514, February 2022. arXiv: 2002.00388.

[7] Daniel Ruffinelli, Samuel Broscheit, and Rainer Gemulla. You CAN Teach an Old Dog New Tricks! On Training Knowledge Graph Embeddings. April 2020.

[8] Mehdi Ali, Max Berrendorf, Charles Tapley Hoyt, Laurent Vermue, Mikhail Galkin, Sahand Sharifzadeh, Asja Fischer, Volker Tresp, and Jens Lehmann. Bringing Light Into the Dark: A

Large-Scale Evaluation of Knowledge Graph Embedding Models Under a Unified Framework. *IEEE Transactions on Pattern Analysis and Machine Intelligence*, 44(12):8825–8845, December 2022.

[9] Danny Sullivan. A reintroduction to our Knowledge Graph and knowledge panels, May 2020.

[10] Zhilin Yang, Zihang Dai, Ruslan Salakhutdinov, and William W. Cohen. Breaking the Softmax Bottleneck: A High-Rank RNN Language Model, 2017. Version Number: 4.

[11] Zhilin Yang, Thang Luong, Ruslan Salakhutdinov, and Quoc Le. Mixtape: breaking the softmax bottleneck efficiently. In *Proceedings of the 33rd International Conference on Neural Information Processing Systems*, number 519, pages 5775–5783. Curran Associates Inc., Red Hook, NY, USA, December 2019.

[12] Sekitoshi Kanai, Yasuhiro Fujiwara, Yuki Yamanaka, and Shuichi Adachi. Sigsoftmax: Reanalysis of the Softmax Bottleneck, 2018. Version Number: 1.

[13] Octavian-Eugen Ganea, Sylvain Gelly, Gary Bécigneul, and Aliaksei Severyn. Breaking the Softmax Bottleneck via Learnable Monotonic Pointwise Non-linearities. 2019. Publisher: arXiv Version Number: 2.

[14] Andreas Grivas, Antonio Vergari, and Adam Lopez. Taming the Sigmoid Bottleneck: Provably Argmaxable Sparse Multi-Label Classification, 2023. Version Number: 2.

[15] Erik Arakelyan, Daniel Daza, Pasquale Minervini, and Michael Cochez. Complex Query Answering with Neural Link Predictors. *arXiv:2011.03459 [cs]*, January 2021. arXiv: 2011.03459.

[16] Erik Arakelyan, Pasquale Minervini, Daniel Daza, Michael Cochez, and Isabelle Augenstein. Adapting Neural Link Predictors for Data-Efficient Complex Query Answering, 2023. Version Number: 3.

[17] Matthew Finlayson, John Hewitt, Alexander Koller, Swabha Swayamdipta, and Ashish Sabharwal. Closing the Curious Case of Neural Text Degeneration, 2023. Version Number: 1.

[18] Andrzej Cichocki, Danilo Mandic, Lieven De Lathauwer, Guoxu Zhou, Qibin Zhao, Cesar Caiafa, and Huy Anh Phan. Tensor Decompositions for Signal Processing Applications: From two-way to multiway component analysis. *IEEE Signal Processing Magazine*, 32(2):145–163, March 2015.

[19] Maximilian Nickel, Volker Tresp, and Hans-Peter Kriegel. A three-way model for collective learning on multi-relational data. In *Proceedings of the 28th International Conference on International Conference on Machine Learning*, ICML'11, pages 809–816, Madison, WI, USA, June 2011. Omnipress.

[20] Bishan Yang, Wen-tau Yih, Xiaodong He, Jianfeng Gao, and Li Deng. Embedding Entities and Relations for Learning and Inference in Knowledge Bases, 2014. Version Number: 4.

[21] Théo Trouillon, Christopher R. Dance, Johannes Welbl, Sebastian Riedel, Éric Gaussier, and Guillaume Bouchard. Knowledge Graph Completion via Complex Tensor Factorization, 2017. Version Number: 2.

[22] Timothée Lacroix, Nicolas Usunier, and Guillaume Obozinski. Canonical Tensor Decomposition for Knowledge Base Completion, 2018. Version Number: 1.

[23] Seyed Mehran Kazemi and David Poole. SimplE Embedding for Link Prediction in Knowledge Graphs, 2018. Version Number: 2.

[24] Ivana Balažević, Carl Allen, and Timothy M. Hospedales. TuckER: Tensor Factorization for Knowledge Graph Completion. 2019. Publisher: arXiv Version Number: 2.

[25] Tim Dettmers, Pasquale Minervini, Pontus Stenetorp, and Sebastian Riedel. Convolutional 2D Knowledge Graph Embeddings, 2017. Version Number: 6.

[26] Ivana Balažević, Carl Allen, and Timothy M. Hospedales. Hypernetwork Knowledge Graph Embeddings. 2018. Publisher: arXiv Version Number: 5.

[27] Mikhail Galkin, Priyansh Trivedi, Gaurav Maheshwari, Ricardo Usbeck, and Jens Lehmann. Message Passing for Hyper-Relational Knowledge Graphs, 2020. Version Number: 1.

[28] Michael Schlichtkrull, Thomas N. Kipf, Peter Bloem, Rianne van den Berg, Ivan Titov, and Max Welling. Modeling Relational Data with Graph Convolutional Networks, 2017. Version Number: 4.

[29] Antoine Bordes, Nicolas Usunier, Alberto Garcia-Duran, Jason Weston, and Oksana Yakhnenko. Translating Embeddings for Modeling Multi-relational Data. In *Advances in Neural Information Processing Systems*, volume 26. Curran Associates, Inc., 2013.

[30] Pouya Pezeshkpour, Yifan Tian, and Sameer Singh. Revisiting Evaluation of Knowledge Base Completion Models. February 2020.

[31] Rudolf Kadlec, Ondrej Bajgar, and Jan Kleindienst. Knowledge Base Completion: Baselines Strike Back, 2017. Version Number: 1.

[32] Yihong Chen, Pasquale Minervini, Sebastian Riedel, and Pontus Stenetorp. Relation Prediction as an Auxiliary Training Objective for Improving Multi-Relational Graph Representations, 2021. Version Number: 1.

[33] Lorenzo Loconte, Nicola Di Mauro, Robert Peharz, and Antonio Vergari. How to Turn Your Knowledge Graph Embeddings into Generative Models, 2023. Version Number: 3.

[34] Geoffrey E Hinton and Richard Zemel. Autoencoders, Minimum Description Length and Helmholtz Free Energy. In *Advances in Neural Information Processing Systems*, volume 6. Morgan-Kaufmann, 1993.

[35] Leland McInnes, John Healy, Nathaniel Saul, and Lukas Großberger. UMAP: Uniform Manifold Approximation and Projection. *Journal of Open Source Software*, 3(29):861, September 2018. Publisher: The Open Journal.

[36] Andreas Grivas, Nikolay Bogoychev, and Adam Lopez. Low-Rank Softmax Can Have Unargmaxable Classes in Theory but Rarely in Practice, 2022. Version Number: 2.

[37] Thomas M. Cover. The Number of Linearly Inducible Orderings of Points in d-Space. *SIAM Journal on Applied Mathematics*, 15(2):434–439, 1967. Publisher: Society for Industrial and Applied Mathematics.

[38] I. J Good and T. N Tideman. Stirling numbers and a geometric ,structure from voting theory. *Journal of Combinatorial Theory, Series A*, 23(1):34–45, July 1977.

[39] Warren D. Smith. D-dimensional orderings and Stirling numbers, 2014.

[40] Thomas M. Cover. Geometrical and Statistical Properties of Systems of Linear Inequalities with Applications in Pattern Recognition. *IEEE Transactions on Electronic Computers*, EC-14(3):326–334, June 1965.

[41] N. Alon, P. Frankl, and V. Rodl. Geometrical realization of set systems and probabilistic communication complexity. In *26th Annual Symposium on Foundations of Computer Science (sfcs 1985)*, pages 277–280, October 1985. ISSN: 0272-5428.

[42] Kristina Toutanova and Danqi Chen. Observed versus latent features for knowledge base and text inference. In *Proceedings of the 3rd Workshop on Continuous Vector Space Models and their Compositionality*, pages 57–66, Beijing, China, 2015. Association for Computational Linguistics.

[43] Ouns El Harzli, Samy Badreddine, and Tarek R. Besold. What's Wrong with Gradient-based Complex Query Answering? 2023.

[44] Cosimo Gregucci, Bo Xiong, Daniel Hernandez, Lorenzo Loconte, Pasquale Minervini, Steffen Staab, and Antonio Vergari. Is Complex Query Answering Really Complex?, 2024. Version Number: 2.

[45] Zhen Wang, Jianwen Zhang, Jianlin Feng, and Zheng Chen. Knowledge Graph Embedding by Translating on Hyperplanes. *Proceedings of the AAAI Conference on Artificial Intelligence*, 28(1), June 2014.

[46] Yankai Lin, Zhiyuan Liu, Maosong Sun, Yang Liu, and Xuan Zhu. Learning Entity and Relation Embeddings for Knowledge Graph Completion. *Proceedings of the AAAI Conference on Artificial Intelligence*, 29(1), February 2015.

[47] Zhiqing Sun, Zhi-Hong Deng, Jian-Yun Nie, and Jian Tang. RotatE: Knowledge Graph Embedding by Relational Rotation in Complex Space, 2019. Version Number: 1.

[48] Ralph Abboud, İsmail İlkan Ceylan, Thomas Lukasiewicz, and Tommaso Salvatori. BoxE: A Box Embedding Model for Knowledge Base Completion, 2020. Version Number: 2.

[49] Sudhanshu Chanpuriya, Cameron Musco, Konstantinos Sotiropoulos, and Charalampos E. Tsourakakis. Node Embeddings and Exact Low-Rank Representations of Complex Networks, 2020. Version Number: 2.

[50] Mehdi Ali, Max Berrendorf, Charles Tapley Hoyt, Laurent Vermue, Sahand Sharifzadeh, Volker Tresp, and Jens Lehmann. PyKEEN 1.0: A Python Library for Training and Evaluating Knowledge Graph Embeddings, 2020. Version Number: 2.

[51] Diederik P. Kingma and Jimmy Ba. Adam: A Method for Stochastic Optimization, 2014. Version Number: 9.

[52] Nitish Srivastava, Geoffrey Hinton, Alex Krizhevsky, Ilya Sutskever, and Ruslan Salakhutdinov. Dropout: A Simple Way to Prevent Neural Networks from Overfitting. *Journal of Machine Learning Research*, 15(56):1929–1958, 2014.

[53] Sergey Ioffe and Christian Szegedy. Batch Normalization: Accelerating Deep Network Training by Reducing Internal Covariate Shift, 2015. Version Number: 3.

[54] Xavier Glorot and Yoshua Bengio. Understanding the difficulty of training deep feedforward neural networks. In *Proceedings of the Thirteenth International Conference on Artificial Intelligence and Statistics*, pages 249–256. JMLR Workshop and Conference Proceedings, March 2010. ISSN: 1938-7228.

A Tensor Notation

We borrow the notation from [18] for tensors and matrices, summarized in Table 4.

Table 4: The tensor notation used throughout the paper.

Notation	Description
$\mathcal{A}, \mathbf{A}, \mathbf{a}, a$	tensor, matrix, vector, scalar
$\mathbf{A} = \begin{bmatrix} \mathbf{a}_1 & \dots & \mathbf{a}_R \end{bmatrix}$	matrix $\mathbf{A}$ with columns $\mathbf{a}_r$
$\mathbf{A} = \begin{bmatrix} \mathbf{a}_1 \\ \vdots \\ \mathbf{a}_R \end{bmatrix}$	matrix $\mathbf{A}$ with rows $\mathbf{a}_r$
$a_{i_1, i_2, i_3, \dots, i_N}$	scalar of tensor $\mathcal{A}$ obtained by fixing all indices
$\mathbf{a}_{:, i_2, i_3, \dots, i_N}$	fiber of tensor $\mathcal{A}$ obtained by fixing all but one index
$\mathbf{A}_{:, :, i_3, \dots, i_N}$	matrix slice of tensor $\mathcal{A}$ obtained by fixing all but two indices
$\mathcal{A}_{:, :, :, i_4, \dots, i_N}$	tensor slice of $\mathcal{A}$ obtained by fixing some indices
$\mathbf{A}_{(n)} \in \mathbb{R}^{I_n \times I_1 I_2 \dots I_{n-1} I_{n+1} \dots I_N}$	mode-n unfolding of $\mathcal{A}$

B Proofs

Theorem 4.1. *Let* $\mathbf{Y} \in \{0, 1\}^{|\mathcal{E}||\mathcal{R}| \times |\mathcal{E}|}$ *be the representation of the KG with subject-relation pairs on the first axis and objects on the second. Let the sign function* $s(x) = 1$ *if* $x > 0$ *and* $s(x) = 0$ *otherwise. Then,* $\mathbf{Y}$ *can be exactly decomposed as* $\mathbf{Y} = s(\mathbf{HE}^\top)$ *where* $\mathbf{H} \in \mathbb{R}^{|\mathcal{E}||\mathcal{R}| \times (2c^+ + 1)}$, $\mathbf{E} \in \mathbb{R}^{|\mathcal{E}| \times (2c^+ + 1)}$, *and* c^+ *is the maximum out-degree across all subject-relation pairs in the KG. The function* $s(\cdot)$ *is applied element-wise.*

Proof. We extend the approach of [49, 41] to the case of rectangular bipartite adjacency matrices $\mathbf{A} \in \{0, 1\}^{N \times M}$, where N represents the number of source nodes and M the number of destination nodes. c denotes the maximum out-degree of any source node. For the setting of Theorem 4.1, we take $N = |\mathcal{E}||\mathcal{R}|$ and $M = |\mathcal{E}|$.

Our goal is to decompose $\mathbf{A}$ by expressing each row $\mathbf{a}_i \in \{0, 1\}^M$ through the equation
$$s(\mathbf{V}\mathbf{x}_i) = \mathbf{a}_i,$$
where

- $s(\cdot)$ is the sign function $s(z) = \begin{cases} 1, & \text{if } z > 0, \\ 0, & \text{if } z \le 0, \end{cases}$

- $\mathbf{V} \in \mathbb{R}^{M \times (2c+1)}$ is a Vandermonde matrix – that is, a matrix with $2c + 1$ geometric progressions for M variables – with M rows associated to the destination nodes, and

- $\mathbf{x}_i \in \mathbb{R}^{2c+1}$ is a vector of polynomial coefficients associated with source node i.

That is, $\mathbf{x}_i$ define the coefficients of a polynomial of degree $2c$ which, evaluated at each destination node $t = 1, \dots, M$, yields a score $p_i(t)$ that determines the sign of the edge between node i and node t.

If we successfully find such coefficients $\mathbf{x}_i$ for each source node $i = 1, \dots, N$ – which will be guaranteed by the degree $2c$ of the polynomial –, then we can reconstruct the entire adjacency matrix $\mathbf{A}$ as
$$\mathbf{A} = s(\mathbf{V}\mathbf{X}^\top),$$
where $\mathbf{X} \in \mathbb{R}^{N \times (2c+1)}$ is the matrix of coefficients $\mathbf{x}_i$ for all source nodes stacked as rows.

Constructing the Vandermonde Matrix We define the Vandermonde matrix $\mathbf{V}$ such that
$$v_{t,j} = t^{j-1}, \quad t = 1, \dots, M, \ j = 1, \dots, 2c+1.$$
That is, evaluating $\mathbf{V}\mathbf{x}_i \in \mathbb{R}^M$ means evaluating the $2c$-degree polynomial $p_i(t)$ at the integers $t = 1, \dots, M$, each integer t representing a destination node.
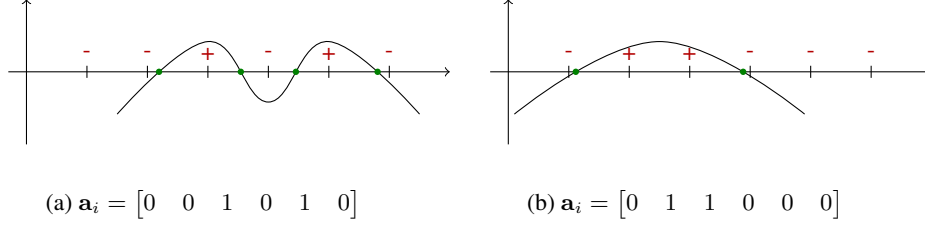
(a) $\mathbf{a}_i = \begin{bmatrix} 0 & 0 & 1 & 0 & 1 & 0 \end{bmatrix}$ (b) $\mathbf{a}_i = \begin{bmatrix} 0 & 1 & 1 & 0 & 0 & 0 \end{bmatrix}$

Figure 3: Fitting a polynomial $p_i(t)$ to the adjacency pattern $\mathbf{a}_i$. The sign of $p_i(t)$ at each integer $t = 1, \ldots, M$ indicates the existence of an edge from i to t. (a) A polynomial with degree $2c$ can always find $2c$ roots (green dots) that isolate the c points where $p_i(t)$ is positive. (b) If the order of the ones in $\mathbf{a}_i$ is such that they form blocks, fewer sign changes are needed.

Fitting the Polynomials   Next, we wish to construct the coefficients $\mathbf{x}_i$ such that the polynomial $p_i(t)$ matches the adjacency pattern $\mathbf{a}_i$:

- $p_i(t) > 0$ for indices where $a_{i,t} = 1$ and

- $p_i(t) < 0$ for indices where $a_{i,t} = 0$.

To achieve this, we choose $p_i(t)$ to have roots at appropriate locations in the intervals between the integer points.

Consider for example the adjacency pattern $\mathbf{a}_i = \begin{bmatrix} 0 & 0 & 1 & 0 & 1 & 0 \end{bmatrix}$. We need $p_i(t)$ to be positive for $t = 3$ and $t = 5$ and negative for all other t. We can choose $p_i(t)$ to have two roots at $t = 3 \pm \epsilon$ and two roots at $t = 5 \pm \epsilon$, where $0 < \epsilon < 1$, and ensuring that the polynomial has positive signs where needed. This is illustrated in Figure 3a.

In general, if the polynomial has degree $2c$, we can always find $2c$ roots that isolate the (at most c) points where $p_i(t)$ is positive. Notice that this requirement is an upper bound. In some cases, the ones in $\mathbf{a}_i$ may appear consecutively (forming blocks) so that fewer sign changes are needed. This particularly likely for graphs with high clustering coefficients, in which case each cluster can be grouped in the ordering (Figure 3b).

Reconstructing the Adjacency Matrix   Once we have determined a coefficient vector $\mathbf{x}_i$ for each source node i, we construct the matrix $\mathbf{X} \in \mathbb{R}^{N \times (2c+1)}$ by stacking them as rows. Then, the entire adjacency matrix can be written as $\mathbf{A} = s(\mathbf{V}\mathbf{X}^\top)$, yielding the desired result.

Interpreting the Embeddings   This decomposition suggests a natural interpretation in terms of node embeddings. Each destination node t corresponds to an object o and is embedded as the vector

$$\mathbf{v}_t = \begin{bmatrix} 1 & t & t^2 & \cdots & t^{2c} \end{bmatrix},$$

corresponding to evaluating the polynomial basis at t. Each source node i corresponds to a subject-relation pair (s, r) and is embedded as the coefficient vector $\mathbf{x}_i$ defining the polynomial $p_i(t)$. The dot product $\mathbf{v}_t^\top \mathbf{x}_i = p_i(t)$ determines the sign at (i, t), i.e., the existence of the triple (s, r, o).

$\square$

C   Subject prediction

Subject prediction is the task of predicting suitable subject entities for $(?, r, o)$ queries. There are conventionally two main approaches to subject prediction with KGE models.

Vector-matrix multiplication   Bilinear models (see Section 2.1) can be used to score all subject entities against a relation-object pair as a vector-matrix multiplication:

$$\mathbf{z}_{:,r,o} = \mathbf{E}\mathbf{h}_{r,o} \tag{5}$$

where $\mathbf{h}_{r,o} \in \mathbb{R}^d$ is an embedded representation of the relation-object pair (r,o) and $\mathbf{E} \in \mathbb{R}^{|\mathcal{E}| \times d}$ is the embedding matrix of all subject entity candidates. For example, in RESCAL's score function $\mathbf{e}_s^\top \mathbf{W}_r \mathbf{e}_o$ [19], we have $\mathbf{h}_{r,o} = \mathbf{W}_r \mathbf{e}_o$, where $\mathbf{W}_r \in \mathbb{R}^{d \times d}$ is a matrix of shared parameters for relation r. In the score function $(\mathbf{e}_s \odot \mathbf{w}_r)^\top \mathbf{e}_o$ of DISTMULT [20], we have $\mathbf{h}_{r,o} = \mathbf{w}_r \odot \mathbf{e}_o$, where $\odot$ is the element-wise (Hadamard) product, and $\mathbf{e}_s, \mathbf{w}_r, \mathbf{e}_o \in \mathbb{R}^d$. Under this perspective, our theoretical results on rank bottlenecks in KGEs for solving object prediction (Section 3) can be extended to subject prediction by replacing the hidden state $\mathbf{h}_{s,r}$ with $\mathbf{h}_{r,o}$. But, our KGE-MoS solution is not applicable simultaneously for both object and subject prediction as the mixture of softmaxes breaks the bilinearity of the score function.

Inverse relations The most general approach which applies to all KGE methods is to introduce inverse relations r^{-1} and to convert the subject prediction query $(?, r, o)$ into an object prediction query $(o, r^{-1}, ?)$ [25, 22]. This introduces $|\mathcal{R}|$ new relations and embeddings, but this parameter count is often negligible compared to the number of parameters of the entities.

$$\mathbf{z}_{:,r,o} := \mathbf{z}_{o,r^{-1},:} = [\mathbf{h}_{o,r^{-1}}] \mathbf{E}^\top \tag{6}$$

In this case, both the theoretical results and the KGE-MoS solution are immediately applicable. We can use the same KGE-MoS layer as follows:

$$P(S|o, r^{-1}) = \sum_{k=1}^{K} \pi_{o,r^{-1},k} \, \mathrm{softmax}(f_k(\mathbf{h}_{o,r^{-1}})\mathbf{E}^\top), \quad \sum_{k=1}^{K} \pi_{o,r^{-1},k} = 1 \tag{7}$$

where S is a random variable that ranges over the same entities as O.

D   Background (cont.)

D.1   Object prediction as a vector-matrix multiplication

In this section, we elaborate on how to rewrite the different KGE models as a function linear in the object embedding $\phi(s,r,o) = \mathbf{h}_{s,r}^\top \mathbf{e}_o$, with $\mathbf{h}_{s,r}, \mathbf{e}_o \in \mathbb{R}^d$.

TUCKER, RESCAL, DISTMULT, CP TUCKER [24] decomposes the score tensor $\mathcal{Z} \in \mathbb{R}^{|\mathcal{E}| \times |\mathcal{R}| \times |\mathcal{E}|}$ as $\mathcal{Z} = \mathcal{W} \times_1 \mathbf{E} \times_2 \mathbf{R} \times_3 \mathbf{E}$ where $\mathcal{W} \in \mathbb{R}^{d \times d_r \times d}$ is a core tensor of shared parameters across all entities and relations and $\times_n$ are mode-n products.[3] $\mathbf{E} \in \mathbb{R}^{|\mathcal{E}| \times d}$, $\mathbf{R} \in \mathbb{R}^{|\mathcal{R}| \times d_r}$ are entity and relation embeddings, respectively. The score function is then $\phi_{\mathrm{TUCKER}}(s,r,o) = \mathcal{W} \times_1 \mathbf{e}_s \times_2 \mathbf{w}_r \times_3 \mathbf{e}_o$. Let $\mathbf{h}_{s,r} = \mathcal{W} \times_1 \mathbf{e}_s \times_2 \mathbf{w}_r \in \mathbb{R}^d$. Then, $\phi_{\mathrm{TUCKER}}(s,r,o) = (\mathbf{h}_{s,r}^{\mathrm{TUCKER}})^\top \mathbf{e}_o$. Specific implementations of the core tensor $\mathcal{W}$ recovers the other bilinear models as special cases.

COMPLEX, SIMPLE As explained by [23, 24], COMPLEX [21] can be seen as a special case of TUCKER and bilinear models by considering the real and imaginary part of the embedding concatenated in a single vector, e.g., $[\mathrm{Re}(\mathbf{e}_o), \mathrm{Im}(\mathbf{e}_o)]^\top \in \mathbb{R}^{2d}$ for the object. We detail this to highlight that the rank bottleneck for these models is $2d$ rather than d. The score function of COMPLEX is

$$\phi_{\mathrm{COMPLEX}}(s,r,o) = (\mathrm{Re}(\mathbf{e}_s) \odot \mathrm{Re}(\mathbf{w}_r))^\top \mathrm{Re}(\mathbf{e}_o) + (\mathrm{Im}(\mathbf{e}_s) \odot \mathrm{Re}(\mathbf{w}_r))^\top \mathrm{Im}(\mathbf{e}_o)$$
$$(\mathrm{Re}(\mathbf{e}_s) \odot \mathrm{Im}(\mathbf{w}_r))^\top \mathrm{Im}(\mathbf{e}_o) - (\mathrm{Im}(\mathbf{e}_s) \odot \mathrm{Im}(\mathbf{w}_r))^\top \mathrm{Re}(\mathbf{e}_o)$$

Let us define $\mathbf{h}_{sr}^1 = \mathrm{Re}(\mathbf{e}_s) \odot \mathrm{Re}(\mathbf{w}_r) - \mathrm{Im}(\mathbf{e}_s) \odot \mathrm{Im}(\mathbf{w}_r)$ and $\mathbf{h}_{sr}^2 = \mathrm{Im}(\mathbf{e}_s) \odot \mathrm{Re}(\mathbf{w}_r) + \mathrm{Re}(\mathbf{e}_s) \odot \mathrm{Im}(\mathbf{w}_r)$, with $\mathbf{h}_{sr}^1, \mathbf{h}_{sr}^2 \in \mathbb{R}^d$. We have

$$\phi_{\mathrm{COMPLEX}}(s,r,o) = (\mathbf{h}_{sr}^1)^\top \mathrm{Re}(\mathbf{e}_o) + (\mathbf{h}_{sr}^2)^\top \mathrm{Im}(\mathbf{e}_o).$$

Concatenating the real and imaginary parts of $\mathbf{e}_o$ into a single vector $\mathbf{e}_o^{\mathrm{COMPLEX}} = [\mathrm{Re}(\mathbf{e}_o), \mathrm{Im}(\mathbf{e}_o)]^\top \in \mathbb{R}^{2d}$, and concatenating the hidden vectors $\mathbf{h}_{sr}^1$ and $\mathbf{h}_{sr}^2$ into a single vector $\mathbf{h}_{sr}^{\mathrm{COMPLEX}} = [\mathbf{h}_{sr}^1; \mathbf{h}_{sr}^2] \in \mathbb{R}^{2d}$, we have

$$\phi_{\mathrm{COMPLEX}}(s,r,o) = (\mathbf{h}_{sr}^{\mathrm{COMPLEX}})^\top \mathbf{e}_o^{\mathrm{COMPLEX}}$$

which is linear in the object embedding $\mathbf{e}_o^{\mathrm{COMPLEX}}$, this time with bottleneck dimension $2d$. A similar trivial result can be done for SIMPLE [23], again considering the concatenation of two embeddings in a single vector in $\mathbb{R}^{2d}$.

---

[3]The mode-n product $\mathcal{X} \times_n \mathbf{A}$ is the tensor obtained by multiplying each slice of $\mathcal{X}$ along the n-th mode by the corresponding column of $\mathbf{A}$. That is, $(\mathcal{X} \times_n \mathbf{A})_{i_1 \ldots i_{n-1} \, j \, i_{n+1} \ldots i_N} = \mathbf{a}_{j,:}^\top \mathbf{x}_{i_1, \ldots, i_{n-1}, :, i_{n+1}, \ldots, i_N}$.

D.2 Output functions in KGEs

In this section, we further detail the different output functions that KGEs parameterized over the years and the loss functions that were used to train them.

Raw scores with margin-based loss (RR)   Early KGEs [29, 20] used margin-based loss functions for ranking reconstruction (RR). The loss ensures that the scores of true triples are higher than the scores of false triples by at least a margin $\gamma > 0$, but does not ensure sign or calibrated reconstruction.

Sigmoid layers with BCE loss (RR, SR, possibly DR)   [21], followed by [25], proposed to use binary cross-entropy (BCE) loss between the scores and the binary representation of the graph. They define a sigmoid layer $P(y_o = 1|\mathbf{h}_{s,r}) = \sigma(\mathbf{h}_{s,r}^\top \mathbf{e}_o)$, where $y_o = 1$ if $(s, r, o) \in \mathcal{G}$ and 0 otherwise. This defines a multi-label classifier with predictions $\hat{\mathbf{y}} = \mathbb{1}(\mathbf{Eh}_{s,r} > 0) \in \{0, 1\}^{|\mathcal{E}|}$ where $\mathbb{1}$ is the indicator function applied element-wise and the i-th entry is the binary prediction for object i. This classifier naturally aligns with sign-label reconstruction (SR). Calibrated scores (DR) were not a concern in this setting until [15, 16] started to combine the binary prediction scores of several simple queries to answer complex queries, which requires the scores to be calibrated.

Softmax layers with CE loss (RR, possibly DR)   [31] proposed to use a cross-entropy (CE) loss. For a query $(s, r, ?)$, they define a vector of probabilities $\mathbf{p}_{s,r} = \mathrm{softmax}(\mathbf{Eh}_{s,r}) \in \Delta^{|\mathcal{E}|}$, with $\Delta^{|\mathcal{E}|}$ the probability simplex over the objects. Here, softmax is applied element-wise to get the components $p_{s,r,o} = \exp(\mathbf{h}_{s,r}^\top \mathbf{e}_o) / \sum_{o' \in \mathcal{E}} \exp(\mathbf{h}_{s,r}^\top \mathbf{e}_{o'})$. This vector should align with the data distribution (labels of the corresponding triples, normalized to sum to 1). Although softmax is typically used for predicting a single correct class, here it is repurposed for multi-label scenarios by retrieving top-k entries and ranking likely completions (RR). This modeling also opens the door to sampling [33] which requires calibrated scores (DR).

In comprehensive benchmarking efforts, [7] and [8] re-evaluated all score functions with all possible output functions and loss functions for ranking reconstruction (RR). They found that softmax-based modeling generally outperform other approaches, closely followed by modeling with BCE loss. Models trained with margin-based loss functions were consistently the worst performing. Note that the authors did not evaluate the performance of models for sign-label reconstruction (SR) or calibrated score reconstruction (DR).

E   Rank bottlenecks in KGEs (cont.)

E.1   Log-linearity of the softmax bottleneck

As we mention in 3.1, the softmax function maps the d-dimensional linear subspace of scores to a smooth d-dimensional manifold within the $(|\mathcal{E}| - 1)$-dimensional probability simplex $\Delta^{|\mathcal{E}|}$. While this manifold is non-linear, its shape is relatively simple and can be described by the following constraint: its composition with the log function is a linear function of the scores. An algebraic perspective on this bottleneck is provided by [10]. Let $\mathbf{A} \in \mathbb{R}^{|\mathcal{E}||\mathcal{R}| \times |\mathcal{E}|}$ be the log-probability matrix where $a_{i,j} = \log P(O = j|\mathbf{h}_i)$. We have

$$\mathbf{A} = \begin{bmatrix} \log \mathrm{softmax}(\mathbf{Eh}_{1,1}) \\ \vdots \\ \log \mathrm{softmax}(\mathbf{Eh}_{|\mathcal{E}|,|\mathcal{R}|}) \end{bmatrix} = \mathbf{HE}^\top - \begin{bmatrix} c_{1,1} \\ \vdots \\ c_{|\mathcal{E}|,|\mathcal{R}|} \end{bmatrix} \begin{bmatrix} 1 & \cdots & 1 \end{bmatrix}$$

where $c_i = \log \sum_{j=1}^{|\mathcal{E}|} \exp(\mathbf{Eh}_i)_j \in \mathbb{R}$ is the log-partition function. Since $\mathbf{HE}^\top$ has a rank at most d, and the term involving log-partition functions has a rank at most 1, the resulting log-probability matrix $\mathbf{A}$ has a rank of at most $d + 1$.
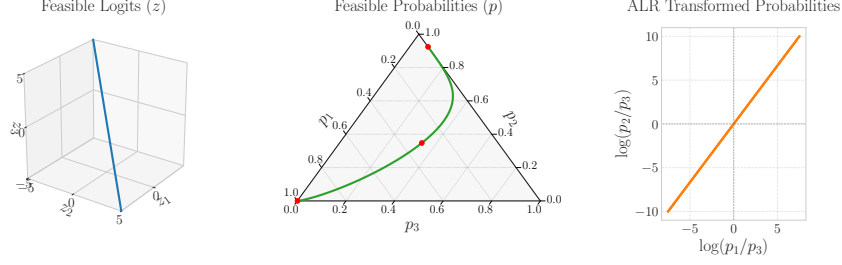
Figure 4: Visualisation of the softmax bottleneck. The blue line is the linear subspace of feasible scores for a fixed matrix $\mathbf{E}$, where each point is calculated for a different hidden state $\mathbf{h}_{s,r}$. The green line is the set of feasible probability distributions after the softmax function, and the orange line is the additive-log ratio of the probabilities. As softmax is log-linear, the feasible distributions are constrained to a manifold that is linear in the ALR space. Any groundtruth that does not respect this constraint cannot be represented by the model.

We can visualise this log-linearity using log-ratio transformations. For example, for a vector of probabilities $\mathbf{p} \in \Delta^{|\mathcal{E}|}$, we use an Additive Log-Ratio (ALR) transformation with $p_{|\mathcal{E}|}$ as the reference:

$$
\text{ALR}(\mathbf{p}) = \begin{bmatrix} \log \frac{p_1}{p_{|\mathcal{E}|}} \\ \vdots \\ \log \frac{p_{|\mathcal{E}|-1}}{p_{|\mathcal{E}|}} \end{bmatrix} \tag{8}
$$

This transformation maps the simplex to a $d-1$ dimensional space where the log-partitions are eliminated in the ratios. As we visualise in Figure 4, the log-ratio of the probabilities span a linear subspace of the possible probability ratios. Any groundtruth that does not respect this log-linear constraint cannot be represented by the model.

F Experiments

F.1 Datasets

We use the usual splits for `FB15K237` [42] and `ogbl-biokg` [4]. `openbiolink` [2] comes with four available datasets. We use the high-quality, directed set downloadable from the PyKeen library[50], which filters out test entities that do not appear in the training set and are not learnable by knowledge graph embedding models. `Hetionet` [1] does not come with pre-defined splits. We obtain the splits via the PyKeen library using a seed of 42. Table 5 reports statistics for all datasets.

Table 5: Dataset statistics and $(s, r, \cdot)$ out-degrees. The sufficient embedding dimension d_{SR}^+ for exact sign reconstruction is calculated based on the maximum out-degree according to Theorem 4.1.

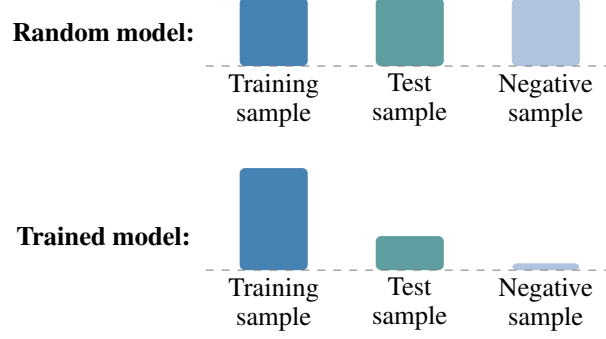| Dataset	#Entities	#Rels	#Triples	Inverse Relations	Out-Degree			d_{SR}^+
					Mean	Median	Max	
FB15k-237	14,541	237	310,116	✗	3.03	1	954	1,909
				✓	3.83	1	4,364	8,729
Hetionet	45,158	24	2,250,197	✗	29.07	7	15,036	30,073
				✓	21.66	6	15,036	30,073
ogbl-biokg	93,773	51	5,088,434	✗	40.54	14	29,328	58,657
				✓	37.48	12	29,328	58,657
openbiolink	180,992	28	4,559,267	✗	14.47	2	2,251	4,503
				✓	18.12	2	18,420	36,841

Figure 5: Likelihood assigned by models to training/test/random samples. Because in KGC the set of training and test samples are disjoint, trained models leave less probability mass for test samples even if the model would assign higher probability to test samples if training samples were not options.

F.2 Metrics

Filtered NLL The negative log-likelihood (NLL) metric measures how well a model assigns probability to the true triples in the test set. However, in KGC, because the training and test sets are disjoint, a model trained to assign high probability to training triples might leave little probability mass for test triples, even if they follow similar patterns. In this case, the NLL can unfairly penalise models that fit the training set well but are able to generalise out-of-distribution, as generalisation in KGC is always *out-of-distribution* rather than in-distribution.

To address this issue, we use a filtered version of NLL when evaluating on the test set. For a $(s, r, ?)$ query, we zero out the probabilities of ground truth objects for that query seen during training, renormalising the probabilities of the model predictions. Formally, given a model prediction $P(o|s, r)$, we define the filtered test probability as

$$P^{\text{filtered}}(o|s, r) = \frac{\mathbb{1}[(s, r, o) \notin \mathcal{G}_{\text{train}}]P(o|s, r)}{\sum_{o' \in \mathcal{E}} \mathbb{1}[(s, r, o') \notin \mathcal{G}_{\text{train}}]P(o'|s, r)} \tag{9}$$

This filtered approach provides a more meaningful evaluation of the model's ability to generalize to unseen triples, as it focuses on the model's ability to distinguish test triples from truly negative samples rather than from training triples that the model has already learned. It prevents situations where a model that accurately assigns high probability to training instances might be unfairly disadvantaged compared to a less informed model when evaluating predictions on the disjoint test set (Figure 5).

Ranking metrics The quality of a KGC model is commonly assessed by ranking the scores of test triples $(s, r, o) \in \mathcal{G}_{\text{test}}$. For example, in the context of object prediction, the ranks are computed as

$$R_\theta(s, r, o) := 1 + \sum_{e \in \mathcal{E}'} \mathbb{1}[\Phi_\theta(s, r, e) > \Phi_\theta(s, r, o)]. \tag{10}$$

where $\mathbb{1}[\cdot]$ is the indicator function and the set $\mathcal{E}' := \{e \in \mathcal{E} \mid (s, r, e) \notin \mathcal{G}\}$ filters the rank by only including object entities that do not form KG triples. A pessimistic version of the rank is sometimes considered by taking a non-strict inequality The mean reciprocal rank (MRR) is the mean of the reciprocal ranks MRR $= \frac{1}{|\mathcal{G}_{\text{test}}|} \sum_{(s,r,o) \in \mathcal{G}_{\text{test}}} R_\theta(s, r, o)^{-1}$. The mean rank (MR) is the arithmetic mean of the ranks, but is notably sensitive to outliers. The Hits@k metric is the proportion of test triples that are ranked within the top k positions.

Notice that in `ogbl-biokg`, each test object for $(s, r, ?)$ are not ranked against all entities, but only against a pre-defined set of 500 entities. The same holds for subject prediction $(?, r, o)$.

F.3 Experimental setting

General Hyperparameters We guide the choice of hyperparameters by guidelines from the original papers of each model, as well as insights from recent benchmarking papers [7, 8]. All baseline models are trained using the Adam optimizer [51] with a learning rate of 10^{-4}, except for DISTMULT, which

uses a higher learning rate of 10^{-3}. We use a batch size of 1000 for all models as KGEs are more stable with larger batch sizes [7], except for RESCAL-MOS, our largest model, which uses a batch size of 500 for memory constraints. The models are trained for 30 training set epochs, with early stopping according to validation set metrics at a patience of 8 epochs.

Regularisation   Following the findings of [7], which showed that dropout [52] is more effective than norm-based regularisation for KGEs, we apply a dropout of 0.1 to the encoded representation $\mathbf{h}_{s,r}$ (recalling that models can be represented as $\phi(s, r, o) = \mathbf{h}_{s,r}^{\top} \mathbf{e}_o$). An exception to this is CONVE, which already incorporates dropout within its neural network layers.

CONVE specific hyperparameters   For CONVE, we adopt the hyperparameter settings from its original paper [25]. The model reshapes the input subject and relation embeddings into two-dimensional "images" (height 8), followed by a two-layer convolutional network with 32 channels and a kernel size of $(3, 3)$. The output is then passed through a fully connected layer to obtain $\mathbf{h}_{s,r}$. Regularisation for CONVE includes dropout on embeddings (0.2), feature maps after convolution (0.3), and the output of the fully connected layer (0.3). Each layer in CONVE is also followed by a batch normalisation layer [53].

KGE-MOS details and hyperparameters   For the KGE-MOS layer, defined as:

$$P(O|s,r) = \sum_{k=1}^{K} \pi_{s,r,k} \operatorname{softmax}(f_k(\mathbf{h}_{s,r})\mathbf{E}^{\top}), \quad \sum_{k=1}^{K} \pi_{s,r,k} = 1 \tag{11}$$

we use two-layer projections for $f_k(\mathbf{h}_{s,r})$, maintaining the same intermediate dimension d as the KGE dimension. Each projection layer is followed by batch normalisation [53], a non-linear activation, and hidden dropout (applied in that order). To encourage the use of all mixture components, we incorporate the entropy of the distribution defined by the mixture weights $(\pi_{s,r,1}, \ldots, \pi_{s,r,K})$ into the loss function. Our hyperparameter search for KGE-MOS involved a random exploration over learning rate (10^{-2} to 10^{-5}, log-scale), hidden dropout (0.0 to 0.2), activation type (ReLU, LeakyReLU, GeLU, tanh), and entropy regularisation weight (10^{-7} to 1.0, log-scale). The final reported results for KGE-MOS were obtained with a learning rate of 10^{-4}, hidden dropout of 0.1, LeakyReLU activation, and an entropy regularisation weight of 10^{-3}.

Parameters initialisation   Parameters for the KGEs and all model layers are initialised using Xavier uniform initialisation [54]. Repeated runs are performed with different initialisation seeds for statistical significance.

Hardware   All experiments are run on NVIDIA A10 GPUs with 24GB of memory. Time of execution for each baseline ranges from a couple of hours for FB15K237, the smallest dataset, to 1-2 days for openbiolink, the largest dataset.

F.4   Additional results

Tables 6, 7, 8 and 9 report the full results for the FB15k-237, Hetionet, ogbl-biokg, and openbiolink datasets, respectively. In Table 10 we report inference time results for all methods.

Table 6: Full results for the FB15k-237 dataset.

Model	FB15k-237						
	NLL↓	MRR↑	MR↓	Hits@1↑	Hits@3↑	Hits@10↑	Param
d = 200							
DISTMULT	4.74±.08	.304±.004	228±7.5	.216±.003	.331±.005	.482±.004	3.0M
DISTMULT-MoS	4.65±.01	.306±.002	214±0.3	.220±.002	.336±.001	.479±.003	3.3M
RESCAL	4.79±.01	.285±.001	246±2.3	.210±.001	.309±.001	.432±.001	21.9M
RESCAL-MoS	4.65±.01	.318±.001	220±1.1	.230±.002	.348±.001	.494±.001	22.2M
CONVE	**4.48±.01**	**.321±.001**	**176±2.6**	**.232±.000**	**.351±.001**	**.499±.001**	5.1M
CONVE-MoS	4.57±.01	.311±.002	203±1.1	.227±.002	.339±.003	.479±.002	5.4M
d = 1000							
DISTMULT	**4.56±.01**	**.331±.001**	208±2.8	**.241±.001**	**.362±.001**	**.514±.003**	15.0M
DISTMULT-MoS	4.72±.00	.311±.001	231±2.3	.221±.003	.341±.000	.492±.002	23.0M
RESCAL	4.64±.00	.307±.001	216±0.7	.221±.001	.335±.003	.483±.002	488.5M
RESCAL-MoS	4.63±.01	.325±.002	259±5.4	.236±.004	.357±.002	.505±.001	496.5M
CONVE	4.65±.04	.301±.001	**185±4.3**	.212±.001	.329±.001	.485±.002	70.1M
CONVE-MoS	4.69±.01	.316±.001	222±1.5	.227±.001	.347±.001	.497±.002	78.2M

Table 7: Full results for the Hetionet dataset.

Model	Hetionet						
	NLL↓	MRR↑	MR↓	Hits@1↑	Hits@3↑	Hits@10↑	Param
d = 200							
DISTMULT	6.10±.00	.250±.001	695±2.4	.176±.001	.274±.001	.395±.001	9.0M
DISTMULT-MoS	**5.83±.00**	**.277±.002**	**488±1.3**	**.202±.003**	**.303±.002**	**.423±.002**	9.4M
RESCAL	6.13±.00	.219±.001	607±0.4	.153±.001	.237±.001	.351±.001	10.9M
RESCAL-MoS	5.87±.01	.274±.000	505±2.0	.200±.000	.300±.001	.419±.001	11.3M
CONVE	6.03±.00	.252±.001	610±2.3	.180±.001	.275±.002	.395±.002	11.1M
CONVE-MoS	5.92±.00	.263±.001	536±1.1	.193±.002	.284±.002	.400±.001	11.4M
d = 1000							
DISTMULT	6.04±.00	.288±.000	633±1.9	.217±.001	.314±.000	.429±.000	45.2M
DISTMULT-MoS	5.76±.00	.312±.001	**491±1.5**	.233±.001	**.344±.001**	**.467±.001**	53.2M
RESCAL	5.93±.00	.243±.001	650±3.6	.165±.001	.270±.001	.398±.001	93.1M
RESCAL-MoS	5.87±.03	.300±.009	542±4.9	.223±.009	.327±.010	.454±.008	101.2M
CONVE	6.06±.00	.262±.001	635±4.7	.187±.001	.288±.001	.411±.001	100.3M
CONVE-MoS	**5.71±.01**	**.313±.001**	505±3.7	**.237±.002**	.343±.001	.462±.001	108.3M

Table 8: Full results for the ogbl-biokg dataset.

Model	ogbl-biokg						
	NLL↓	MRR↑	MR↓	Hits@1↑	Hits@3↑	Hits@10↑	Param
d = 200							
DISTMULT	4.83±.01	.792±.001	5.60±0.1	.713±.001	.849±.001	**.935±.001**	18.8M
DISTMULT-MoS	**4.65±.00**	**.792±.001**	**5.32±0.0**	**.716±.002**	**.844±.000**	.930±.000	19.1M
RESCAL	4.89±.00	.763±.001	6.01±0.0	.679±.001	.818±.001	.917±.000	22.8M
RESCAL-MoS	4.70±.00	.780±.001	5.47±0.0	.699±.001	.835±.001	.928±.000	23.2M
CONVE	4.94±.00	.782±.001	5.57±0.0	.701±.002	.838±.001	.928±.000	20.8M
CONVE-MoS	4.77±.01	.768±.002	5.77±0.1	.683±.003	.824±.002	.923±.001	21.2M
d = 1000							
DISTMULT	4.89±.02	.801±.002	5.96±0.1	.726±.003	.855±.002	.936±.001	93.9M
DISTMULT-MoS	**4.34±.00**	**.837±.001**	**4.51±0.0**	**.772±.002**	**.884±.000**	**.951±.000**	101.9M
RESCAL	4.74±.00	.799±.001	5.66±0.0	.723±.001	.851±.000	.939±.000	195.8M
RESCAL-MoS	4.42±.01	.824±.004	4.87±0.1	.755±.005	.874±.002	.947±.001	203.8M
CONVE	4.93±.00	.807±.000	5.25±0.0	.731±.001	.863±.000	.941±.000	149.0M
CONVE-MoS	4.43±.00	.817±.001	5.17±0.1	.744±.001	.872±.000	.946±.000	157.0M

Table 9: Full results for the openbiolink dataset.

Model	openbiolink						
	NLL↓	MRR↑	MR↓	Hits@1↑	Hits@3↑	Hits@10↑	Param
$d = 200$							
DISTMULT	5.14±.00	.302±.002	1120±10.6	.195±.004	.342±.000	.530±.000	36.2M
DISTMULT-MOS	**5.03±.01**	.314±.001	966±33.4	.207±.001	.351±.001	.543±.000	36.5M
RESCAL	5.16±.00	.303±.001	960±2.20	.197±.002	.339±.001	.527±.001	38.4M
RESCAL-MOS	5.04±.01	**.323±.005**	949±78.8	**.217±.004**	**.361±.005**	**.547±.005**	38.8M
CONVE	5.28±.02	.286±.000	**794±17.6**	.181±.001	.320±.002	.509±.002	38.3M
CONVE-MOS	5.10±.01	.304±.002	967±47.9	.200±.002	.340±.003	.528±.002	38.6M
$d = 1000$							
DISTMULT	5.17±.02	.316±.004	1210±21.2	.209±.004	.357±.003	.541±.004	181.0M
DISTMULT-MOS	**4.89±.01**	**.347±.000**	**799±32.1**	**.236±.002**	**.392±.002**	**.579±.002**	189.0M
RESCAL	5.03±.00	.328±.002	1330±26.6	.222±.002	.366±.001	.552±.002	237.0M
RESCAL-MOS	5.00±.01	.330±.003	1210±27.8	.220±.003	.373±.003	.559±.004	245.0M
CONVE	5.24±.00	.308±.001	1140±24.2	.201±.001	.348±.001	.535±.001	236.2M
CONVE-MOS	4.91±.01	.336±.000	881±22.4	.227±.001	.378±.000	.565±.001	244.2M

Table 10: Inference and backpropagation time for a single minibatch on openbiolink at $d = 1000$. RESCAL and RESCAL-MOS are compared at batch size 500 to fit on device memory. Other models are compared at batch size 1000.

Model	Time per batch (ms)
DISTMULT	1.34
DISTMULT-MOS ($K = 1$)	3.30
DISTMULT-MOS ($K = 4$)	3.69
RESCAL	1.51
RESCAL-MOS ($K = 1$)	3.49
RESCAL-MOS ($K = 4$)	3.42
CONVE	2.72
CONVE-MOS ($K = 1$)	4.74
CONVE-MOS ($K = 4$)	4.60